Mice That Lack Thrombospondin 2 Display Connective Tissue Abnormalities That Are Associated with Disordered Collagen Fibrillogenesis, an Increased Vascular Density, and a Bleeding Diathesis

Themis R. Kyriakides,* Yu-Hong Zhu,* Lynne T. Smith,‡ Steven D. Bain,§ Zhantao Yang,* Ming T. Lin,* Keith G. Danielson,‖ Renato V. Iozzo,‖ Mary LaMarca,¶ Cindy E. McKinney,¶ Edward I. Ginns,¶ and Paul Bornstein*‡

*Department of Biochemistry, ‡Department of Medicine, University of Washington, Seattle, Washington 98195; §Zymogenetics, Inc., Seattle, Washington 98105; ‖Department of Pathology, Anatomy, and Cell Biology, Jefferson Medical College, Thomas Jefferson University, Philadelphia, Pennsylvania 19107; and ¶Clinical Neuroscience Branch, National Institute of Mental Health, National Institutes of Health, Bethesda, Maryland 20892

Abstract. Thrombospondin (TSP) 2, and its close relative TSP1, are extracellular proteins whose functions are complex, poorly understood, and controversial. In an attempt to determine the function of TSP2, we disrupted the *Thbs2* gene by homologous recombination in embryonic stem cells, and generated TSP2-null mice by blastocyst injection and appropriate breeding of mutant animals. *Thbs2*−/− mice were produced with the expected Mendelian frequency, appeared overtly normal, and were fertile. However, on closer examination, these mice displayed a wide variety of abnormalities. Collagen fiber patterns in skin were disordered, and abnormally large fibrils with irregular contours were observed by electron microscopy in both skin and tendon. As a functional correlate of these findings, the skin was fragile and had reduced tensile strength, and the tail was unusually flexible. Mutant skin fibroblasts were defective in attachment to a substratum. An increase in total density and in cortical thickness of long bones was documented by histology and quantitative computer tomography. Mutant mice also manifested an abnormal bleeding time, and histologic surveys of mouse tissues, stained with an antibody to von Willebrand factor, showed a significant increase in blood vessels. The basis for the unusual phenotype of the TSP2-null mouse could derive from the structural role that TSP2 might play in collagen fibrillogenesis in skin and tendon. However, it seems likely that some of the diverse manifestations of this genetic disorder result from the ability of TSP2 to modulate the cell surface properties of mesenchymal cells, and thus, to affect cell functions such as adhesion and migration.

THROMBOSPONDIN (TSP)[1] 2 is a member of a family of five, secreted, modular glycoproteins whose functions in the extracellular matrix are diverse and poorly understood (Frazier, 1991; Adams and Lawler, 1993; Bornstein and Sage, 1994; Bornstein, 1995). TSP1 and TSP2 are structurally more similar to each other than to TSPs 3–5 and are, therefore, considered to constitute a subfamily; the two proteins have an identical domain structure and are secreted as disulfide-bonded homotrimers (Bornstein et al., 1991*b*; Bornstein, 1992; Laherty et al., 1992; Bornstein and Sage, 1994). This similarity in structure is reflected in the finding that both TSP1 and TSP2 interact with a number of the same cell surface receptors, including heparan sulfate proteoglycans, low density lipoprotein-related receptor protein (LRP), and the integrin $\alpha_v\beta_3$ (Chen et al., 1994, 1996).

Despite the high degree of similarity in the coding regions of *Thbs2* and *Thbs1*, the DNA sequences of the two promoters are very different. As a result, *Thbs2* does not display the rapid transcriptional responses to growth factors, such as PDGF and basic FGF, and to serum, that were observed for *Thbs1* (Bornstein et al., 1991*a*; Bornstein, 1992). The two genes also respond differently to

Address all correspondence to Paul Bornstein, Department of Biochemistry, Box 357350, University of Washington, Seattle, WA 98195. Tel.: (206) 543-1789. Fax: (206) 685-4426. E-mail: bornsten@u.washington.edu

1. *Abbreviations used in this paper*: EDS, Ehlers-Danlos syndrome; ES, embryonic stem; H&E, hematoxylin and eosin; LRP, lipoprotein-related receptor protein; pQCT, peripheral quantitative computer tomography; TSP, Thrombospondin; vWF, von Willebrand factor.

ACTH treatment in bovine adrenocortical cells (Lafeuillade et al., 1996) and during osteoblast differentiation of MC3T3-E1 cells (Sherbina and Bornstein, 1992). Finally, the transcripts for each of the two genes display characteristic spatial and temporal distribution patterns in the developing mouse embryo (Iruela-Arispe et al., 1993).

As is true for TSP1, the biological role of TSP2 remains elusive. TSP2 mRNA, as detected by in situ hybridization in mouse (Iruela-Arispe et al., 1993) and chick embryos (Tucker, 1993), appears predominantly in connective tissues such as dermis, tendon, ligament, perichondrium, and pericardium; it is also present in smooth muscle and endothelial cells. However, the function of TSP2 in these tissues and cells, and elsewhere, remains unclear. It has been shown that TSP2 inhibits the angiogenic activity of basic FGF (Volpert et al., 1995) and the formation of focal adhesions in bovine aortic endothelial cells (Murphy-Ullrich et al., 1993). TSP2 is also capable of inhibiting the spreading of bovine adrenocortical cells (Pellerin et al., 1994).

In an effort to understand the biological role of TSP2, we disrupted the *Thbs2* gene in murine embryonic stem cells and generated homozygous TSP2-null mice. *Thbs2* −/− mice, which lack normal TSP2 mRNA and protein, were produced with the expected Mendelian frequency, were normal in appearance, and reproduced normally. However, these animals displayed structural and functional abnormalities in a variety of connective tissues, including skin, tendon, bone, and blood vessels, and mutant skin fibroblasts were defective in attachment to a substratum. Interestingly, collagen fibrils in both skin and tendon were abnormal in size and contour when viewed in the electron microscope. These changes are reminiscent of the abnormalities in collagen fibril structure seen in the human genetic disorder, Ehlers-Danlos syndrome (EDS) I (Vogel et al., 1979), in which mutations in the fibril-associated type V collagen have been found (Burrows et al., 1996), and in EDS IV, which results from defects in type III collagen (Byers, 1995; Smith et al., 1997). Targeted disruptions of types V and III collagens in mice produce more severe versions of these phenotypes (Andrikopoulos et al., 1995; Liu et al., 1997). Abnormal collagen fibrils are also seen in EDS VII, which can result either from mutations in type I collagen chains that hinder the action of procollagen *N*-proteinase, or from defects in the proteinase itself (Byers, 1995). Recently, targeted disruption of the collagen fibril-associated proteoglycan, decorin, which is known to modulate fibril size (Iozzo and Murdoch, 1996), generated mice with fragile skin and collagen fibrils of abnormal size and shape (Danielson et al., 1997).

TSP1 has been shown to bind to a number of collagens; highest affinity binding was seen with type V collagen and was sensitive to calcium ion concentration (Mumby et al., 1984; Galvin et al., 1987). On the other hand, collagen-binding studies have not been reported for TSP2 and neither protein is known to serve as an integral structural component of collagen fibrils. Similarly, the abnormality in bone and the bleeding defect observed in mice lacking TSP2 were unexpected. The findings in TSP2-null mice, therefore, raise a number of fundamental questions relating to cell–matrix interactions, collagen fibrillogenesis, and matrix assembly, questions that we have answered in part by an investigation of the mice described in this report.

Materials and Methods

Construction of Targeting Vector, Homologous Recombination in Embryonic Stem (ES) Cells, and Generation of Mutant Mice

A 129 mouse genomic λ phage library was screened with a 444-bp fragment from the 5′ end of mouse *Thbs2* cDNA, and several positive phage were identified and plaque-purified. A 13-kb genomic fragment, extending from intron I to intron IX, was cloned in pGEM5. This fragment was modified in successive steps to yield a 4.8-kb genomic fragment containing 1.5 kb of sequence 5′ and 3.3 kb of sequence 3′ to a deletion of ~2.6 kb. The deleted segment included exon 2, which contains the translation start site, and exon 3 of the gene. A *PGK-Neo* cassette was then inserted at the site of the deletion. Finally, a *PGK-TK* cassette was cloned 5′ to the 1.5-kb genomic sequence to yield the targeting vector (see Fig. 1 *A*).

J1 ES cells (129/SvJ; a gift of R. Jaenisch, Massachusetts Institute of Technology, Boston, MA) and RW4 ES cells (129/SvJ; Genome Systems, St. Louis, MO) were cultured on neomycin-resistant fibroblasts in DME (high glucose) supplemented with 15% fetal calf serum (ES-qualified; GIBCO BRL, Gaithersburg, MD), 0.1 mM β-mercaptoethanol, 2 mM L-glutamine, 100 U/ml penicillin G, 100 μg/ml streptomycin, and 1,000 U/ml of leukemia inhibitory factor (GIBCO BRL). Cells (10^7) were electroporated with 30 μg of TSP2 targeting vector that was linearized with KpnI. Selection with G418 and gancyclovir was started 24 and 72 h after electroporation, respectively, and resistant clones were picked typically 9–10 d later. DNA was extracted from expanded clones as described by Laird et al. (1991), digested with BamHI, and analyzed by Southern blotting. The genomic probe encompassed 500 bp of DNA 5′ to the *Thbs2* sequence present in the targeting vector and detected a 6- or 4.8-kb BamHI fragment, derived from a wild-type or a targeted allele, respectively (see Fig. 1 *A*).

Correctly targeted ES cells were microinjected into C57BL/6 mouse blastocysts and the resulting male chimeras were mated with C57BL/6 females. Agouti progeny were genotyped by Southern blot analysis of tail DNA. Heterozygous offspring were then bred to homozygosity. Subsequently, chimeras derived from both J1 and RW4 ES cells were mated with 129/SvJ females, and germline heterozygous animals were mated to produce homozygous TSP2-null mice in a homogeneous 129 background.

RNA and Protein Extraction: Northern and Western Blots

Extraction of RNA from 18-d-old embryos and fibroblasts was carried out by the guanidinium thiocyanate method (Chomczynski et al., 1987). RNA was separated on 1% agarose gels containing 2.2 M formaldehyde. For Western blots, protein was extracted from 18-d-old embryos after removal of the head and viscera. Tissues were homogenized in a Dounce glass homogenizer in cold extraction buffer (1% NP-40, 150 mM NaCl, 50 mM Tris-HCl, pH 8.0, 3 mM $CaCl_2$, 100 μg/ml phenylmethylsulfonyl fluoride, 1 μg/ml pepstatin A, and 0.5 μg/ml leupeptin). The resulting homogenate was centrifuged at 3,000 rpm for 5 min at room temperature and heated at 95°C for 5 min. Protein concentration was assayed by absorbance at 595 nm with a protein assay reagent (Bio-Rad Laboratories, Cambridge, MA), and equal amounts of protein were separated on a 7% polyacrylamide gel. After transfer to Zetabind membrane (Cuno Inc., Meriden, CT) for 1 h at 100 V, the membrane was air-dried for 30 min in the dark and blocked for 1 h with 5% nonfat milk in PBS plus 0.3% Tween-20. The membrane was then incubated in PBS with anti–mouse TSP2 antibody. Two antibodies produced similar results; one was generated in a guinea pig against the amino-terminal region of mouse TSP2, (amino acids 1–296, including the heparin-binding domain), and the other (a kind gift of D. Mosher, University of Wisconsin, Madison, WI), in rabbits against intact TSP2. Both antigens were generated in a baculovirus expression system. The membrane was washed further with PBS and then incubated with an anti–rabbit or anti–guinea pig IgG–biotin conjugate. The resulting antigen–antibody complexes were detected by incubation in A and B reagent (BioRad Laboratories, Hercules, CA).

Tissue Sampling, Histology, Immunolocalization, and Electron Microscopy

Soft tissues were dissected, fixed in 10% buffered formalin, and processed for histological examination by light microscopy. The femurs and tibias

were excised, dissected to the periosteum, and fixed in 70% ethanol. The right femurs and tibias were then reserved for bone density determinations, whereas the bones in the left leg were fixed afterwards in phosphate-buffered formalin and were processed for histology. After formalin fixation, the diaphyseal samples of long bones were demineralized in buffered formic acid (equal proportions of 5% formic acid and 20% sodium citrate, pH 4.2), washed, partially dehydrated in 70% ethanol, and embedded in paraffin. 4 μm sections were cut with a Reichert Jung rotary microtome, mounted on glass slides, and stained with hematoxylin and eosin (H & E). Soft tissue sections were stained with Verhoeff-van Gieson, orcein, or H & E stains, according to standard procedures.

For immunolocalization of TSP2, paraffin sections of skin from the back of 3-mo-old mice were heated at 60°C for 15 min, dewaxed in xylene, and rehydrated through a graded series of ethanol. Subsequently, the sections were treated with 3% H_2O_2, 0.1% sodium azide in methanol, blocked with 1% BSA in PBS, and then incubated with anti-TSP2 antibody at a 1:1,000 dilution. Detection of TSP2-specific immunoreactivity was achieved with an Elite ABC kit (Vector Labs, Inc., Burlingame, CA), according to the suppliers instructions. After development of peroxidase activity, sections were counterstained with methyl green for 30 s, dehydrated through a graded series of ethanol, mounted with Cytoseal 60 (Stephens Scientific, Riverdale, NJ), and examined with the aid of a Nikon Eclipse 800 microscope.

For immunolocalization of von Willebrand factor (vWF), paraffin sections were dewaxed and rehydrated as described above, and then treated with 0.2% Tween-20 in PBS for 30 min, followed by treatment with a 1:1 solution of 0.25% trypsin (GIBCO BRL) and 0.025% pronase (Sigma Chemical Co., St. Louis, MO; P-8038) for 10 min at 37°C. The sections were then blocked with 10% goat serum at 4°C overnight. After incubation in anti-vWF antibody (Dako Corp., Carpinteria, CA) at 1:500 dilution, the sections were incubated sequentially in anti–rabbit biotin-conjugated antibodies, 3% hydrogen peroxide/0.15% sodium azide/0.05% Tween-20 in PBS, avidin-biotin-peroxidase reagent, and diamino-benzidine substrate (Vector Labs, Inc.), with PBS washes (two washes for 5 min each) between each step. After visualization of the specific peroxidase activity, the sections were counterstained in Gill's No. 2 hematoxylin, and dehydrated and mounted as described above.

All sections stained with anti-vWF antibodies were number coded to allow investigators to perform blind analyses. For transverse sections of embryos, sections were chosen from the same areas of the embryo, as indicated by the appearance of tissues such as thymus, the arch of the aorta, and the limbs. For neonatal and adult tissues, the skin sections were chosen from the lower back of the mouse and, after processing, were embedded and sectioned in a consistent orientation. For analysis, the number of vessels were scored with the aid of a Nikon Eclipse 800 microscope using the 40× objective and the photographic eyepiece. The visible area was calculated to be 0.075 mm^2 with the aid of a 2-mm graded guide. Each sample was scored twice; depending on the size and number of available sections, 7–20 0.075 mm^2 areas were scored per sample.

Samples of skin, including the panniculus carnosus, were removed from the back and shoulder regions, and fixed in 0.1 M sodium cacodylate buffer containing 2.5% glutaraldehyde and 2% paraformaldehyde. The tissue was processed for electron microscopy as previously described (Smith et al., 1997). The magnification of electron micrographs was calibrated with a carbon replica containing 2,160 lines per mm (Ernest F. Fullam, Latham, NY). Electron micrographs of collagen fibril cross-sections were taken at 30,000× magnification. Micrographs were digitized at 72 dpi using an Epson 1200 scanner with Adobe Photoshop 3.0 and Scantastics. The images were transferred into NIH image version 1.52, treated by thresholding, binarized, and analyzed for fibril area and perimeter length. The data were transferred to Excel, and fibril diameters were calculated using $2\sqrt{(\text{area}/\pi)}$. To determine the diameters of skin collagen fibrils, micrographs were taken from the skin of several *Thbs2*−/− and *Thbs2*+/+ animals at 30,000× magnification. A total of 1,090 collagen fibrils were measured using NIH Image software, and histograms were generated.

Measurements by Peripheral Quantitative Computer Tomography (pQCT)

To evaluate bone density changes, pQCT scans using a Norland/Stratec XCT 960M instrument were performed at the distal femur and at the midshafts of the femur and tibia. The total bone density and trabecular density (mg/cm^3) at each site were determined from transverse scans of 0.5 mm thickness. In addition, midshaft cortical thicknesses were calculated from computer-generated algorithms based on cross-sectional geometries. The measurement site for the distal femur was taken as a point halfway between the distal condyle and the midshaft of the diaphysis. The midshaft was the midpoint on the diaphysis. In both instances, the sampling sites were established from bone length measurements determined from pQCT scout views of individual samples.

Analysis of Skin Tensile Strength

The tensile strength of skin from *Thbs2* +/+, *Thbs2* −/−, and decorin −/− mice (which served as a positive control) was analyzed as previously described (Danielson et al., 1997), with the following modifications. Tensile strength measurements of dorsal skin samples were performed with a tabletop tensile-testing machine (Model T-5000; Satec Systems, Inc., Grove City, PA). To avoid slippage, the samples were gripped between clamps equipped with adhesive lycra-covered pads. Skin specimens were stretched at a constant speed of 10 mm/min until failure.

Skin Fibroblasts: Isolation, Culture, and Attachment Assays

Skin fibroblasts were isolated by explant culture of biopsies taken from the backs of adult or neonatal mice. Specimens were cut into 1 mm^2 fragments and allowed to adhere to the surface of 35 mm plates for 5 min. DME, supplemented with 10% fetal calf serum, 2 mM L-glutamine, 100 U/ml penicillin G, 100 μg/ml streptomycin, and 0.25 μg/ml fungizone, was added to dishes, and the medium was changed periodically until the explant-derived cells had become confluent. After two subcultures, the cell population appeared, morphologically, to be composed entirely of fibroblasts.

Attachment assays were performed by modifications of the method of Aumailley et al. (1989). Confluent skin fibroblasts in culture were trypsinized and resuspended in DME containing 10% fetal bovine serum. The cell suspension was adjusted to a final concentration of 2×10^5 cells/ml, 100 μl of each cell type was plated in four wells of a 96-well tissue culture plate, and the plates were incubated at 37°C for 60 min. Wells were either untreated or coated overnight at 4°C with 100 μl/well of TSP2, vitronectin, or fibronectin, each at 5 μg/ml in PBS. Type I collagen was coated in 0.01 N HCl. In addition, a separate aliquot of cells was plated in 60 mm dishes and, after a 60-min incubation at 37°C, the unattached cells, ~50 % of the number plated, were collected and used in the same attachment assay in separate 96-well tissue culture plates. Unattached cells in the 96-well tissue culture plates were removed by washing the plates with DME. Attached cells were fixed with 10% formalin in saline for 30 min and were stained for 30 min with 50 μl/well of 1% methylene blue in 100 mM Tris-HCl buffer, pH 8.0. The plates were then destained for 15 min. After air-drying, the methylene blue that had adsorbed onto the attached cells was solubilized with 0.2% Triton X-100 (50 μl/well). Color yields were measured at 650 nm in a microplate reader. Linearity between optical density and the number of cells attached to a plate was demonstrated by a proportional increase in optical density over an eightfold range in cell concentration.

Determination of Bleeding Time

3-mo-old male mice were used to determine bleeding times. Mice were restrained in a 50-ml falcon tube with holes in its tip and cap. The tail was passed through the cap and a 1-cm segment from the tip of the tail was excised with a sharp razor blade. The tail was kept at the level of the heart during the experiment. Bleeding was monitored by gently absorbing the bead of blood on the tail with a Kimwipe, with care taken not to allow contact with the wound site. Cessation of bleeding was determined by an investigator with no knowledge of the mouse genotype, and was scored to the nearest 0.5 min interval. All experiments were performed at room temperature.

Results

Generation of TSP2-null Mice, Initial Characterization, and Phenotype

To disrupt the TSP2 gene by homologous recombination, J1 and RW4 ES cell lines were electroporated with a targeting construct (Fig. 1 *A*), and selected in G418 and gan-

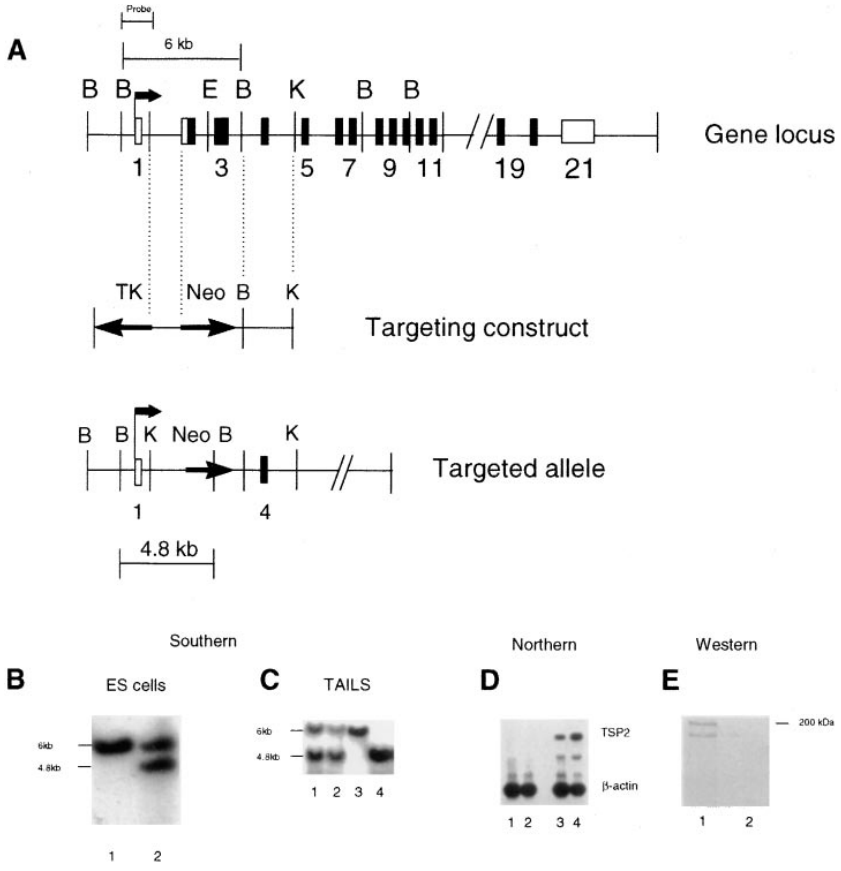

Figure 1. Disruption of the *Thbs2* gene and characterization of TSP2-null mice. (*A*) Targeting strategy. A schematic representation of the *Thbs2* gene locus is shown on the first line. The targeting construct consists of a *PGK-TK* cassette, and 1.5 and 3.3 kb of genomic sequence (*dotted vertical lines*) flanking a *PGK-Neo* cassette. The directions of transcription of the TK and Neo genes are indicated by the bold arrows. In the targeted allele, the *PGK-Neo* cassette replaces 2.6 kb of genomic DNA, which contains exons 2 and 3 of the gene. Angled arrows indicate the start of transcription of *Thbs2*, and open and filled boxes represent untranslated and translated exons, respectively. *B*, BamHI; *E*, EcoRI; *K*, KpnI. (*B*) Southern analysis of BamHI digests of DNA from electroporated ES clones. The probe (*A*, *top*) detects a 6-kb fragment in a digest of a wild-type clone (lane *1*), and bands of 6 kb and 4.8 kb in a digest of a targeted clone (lane *2*). (*C*) Southern analysis of tail DNA from the progeny of Thbs2 +/− mice, analyzed as in *B*. The pattern of 6.0- and 4.8-kb bands indicates that the animals analyzed in lanes *1* and *2* are *Thbs2* +/−, that in lane *3* is *Thbs2* +/+, and that in lane 4 is *Thbs2* −/−. (*D*) Northern blot analysis of RNA prepared from cultured embryonic fibroblasts. Hybridization was performed with a ^{32}P-labeled 515-bp *Thbs2* cDNA probe (nucleotides 834–1,348), or with a β-actin cDNA probe. Lanes *1* and *2* were loaded with 5 and 10 μg of fibroblast RNA, respectively, derived from a *Thbs2* −/− embryo. Lanes *3* and *4* were loaded with 5 and 10 μg, respectively, of fibroblast RNA derived from a *Thbs2* +/+ embryo. The faster migrating transcript has been observed by us and others in the past; its nature is unknown. (*E*) Immunoblot analysis of protein (50 μg) extracted from 17-d-old embryos. An anti-TSP2 antibody was used. Lane *1*, protein from a *Thbs2* +/+ embryo. A band migrating at the expected molecular mass 200 kD is observed. A faster migrating band is also present and is likely to represent a proteolytic fragment of TSP2 since its presence and intensity were variable. Lane *2*, protein from a *Thbs2* −/− embryo. The same samples were immunoblotted with anti-TSP1 antibodies and the presence of approximately equal levels of a TSP1-specific band was evident in both samples (data not shown).

cyclovir. Surviving cell colonies were screened by Southern blotting (Fig. 1 *B*). A frequency of homologous recombination of 10 and 2%, respectively, was observed with the two cell lines. Correctly targeted clones were subsequently screened by Southern blotting with a probe specific for the *PGK-Neo* cassette to exclude the possibility of an additional nonhomologous recombination event (data not shown).

Cells from several correctly targeted ES cell clones were injected into C57BL/6 blastocysts that were subsequently introduced into pseudopregnant foster mothers. Several male chimeras transmitted the disrupted TSP2 allele through the germline. For this study we used a chimera with a 50% degree of chimerism by coat color, derived from a J1 cell clone, and a 95% chimera from an RW4 cell clone. The J1-derived chimera was initially bred with C57BL/6 females; subsequently, both chimeras were bred with 129/SvJ females to achieve a homogeneous 129 background for the mutation.

When a total of 160 offspring of heterozygous *Thbs2* +/− matings were genotyped by Southern blotting (Fig. 1 *C*), the expected Mendelian ratio of 39 +/+, 82 +/−, and 39 −/− animals was observed. Thus, TSP2 is not essential for blastocyst implantation or embryonic development. *Thbs2* −/− mice appeared normal on superficial examination and were able to reproduce normally. A higher incidence of sporadic deaths of adult animals within the TSP2-null population has been observed, but a specific cause of death of these animals has not been determined. As mutant mice aged, a proportion developed a mild kyphosis which appeared to result from lax ligaments rather than from a bony abnormality. The absence of TSP2 mRNA and of immunoreactive protein in *Thbs2* −/− mice was demonstrated by Northern blot and immunoblot analyses, respectively, of embryonic tissue (Fig.1, *D* and *E*). The absence of full-length *Thbs2* mRNA was also shown by reverse transcriptase-PCR assays with primers specific for sequences 5′ and 3′ to the *PGK-Neo* insert (data not shown), and immunohistochemical analysis of both embryonic and adult tissues with anti-TSP2 antibodies confirmed the lack of TSP2 protein (see below). However, on overexposure of Northern blots of RNA from neonatal and embryonic mutant fibroblasts, a band of ~5.3 kb was observed. The size of this band is consistent with the possibility that the neomycin cassette was spliced out, yielding an mRNA that lacks exon 2, with its translation start site,

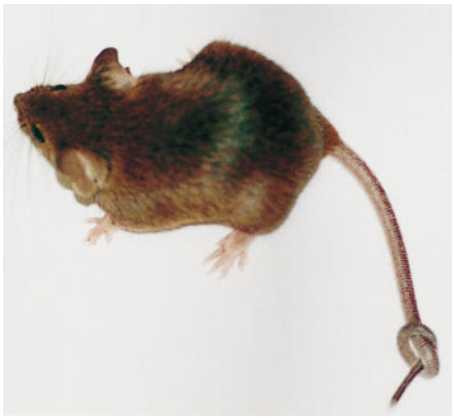

Figure 2. Appearance of the TSP2-null mouse. Disruption of the *Thbs2* gene does not alter the gross appearance of the mouse, but the increased flexibility of tail tendons and ligaments permits the tying of a knot in the tail. This manipulation is not possible in a normal mouse.

and exon 3. This possibility was supported by the results of reverse transcriptase-PCR on this RNA (results not shown). However, this aberrant minor mRNA species is apparently not translated from a downstream ATG in the TSP2 reading frame. To determine whether TSP2-null mice upregulated the expression of the closely related *Thbs1* gene, Northern analyses of RNA extracted from 17-d-old embryos and from neonatal skin fibroblasts were performed. Little or no compensatory increase in expression of *Thbs1* was observed in either case (data not shown).

The phenotype of TSP2-null adult mice derived from the J1 clone, in a mixed 129/SvJ and C57BL/6 background, is characterized by moderate skin fragility, lax tendons and ligaments, an increase in bone density, an increased density of medium and small blood vessels, and a bleeding diathesis. Light and electron microscopy of skin, and electron microscopy of tendon indicated abnormalities in collagen fibers and fibrils. Histology and computerized tomography documented the increase in bone density. Some features of this phenotype are shown in Figs. 2 and 3. Preliminary examination of mutant mice derived from the RW4 ES cell clone, in a pure 129 background, has identified no discrepancies and confirmed several features of this phenotype, including abnormal dermal collagen fibrils, increased vascularity of the dermis and subdermal adipose tissue, and increased bleeding time.

TSP2-null Mice Exhibit a Striking Abnormality in Skin

Although the skin coat and nails of TSP2-null mice appeared normal, an increase in skin laxity and fragility was occasionally noted during handling of the mice. These findings were supported by an increased incidence of superficial lacerations in the mutant colony, presumably resulting from fighting. To determine whether an anatomical basis existed for the increased fragility, skin was sampled from the back, flank, and leg of TSP2-null and wild-type mice, and was examined by light microscopy. A disorganized collagen fiber weave and an abnormal packing of

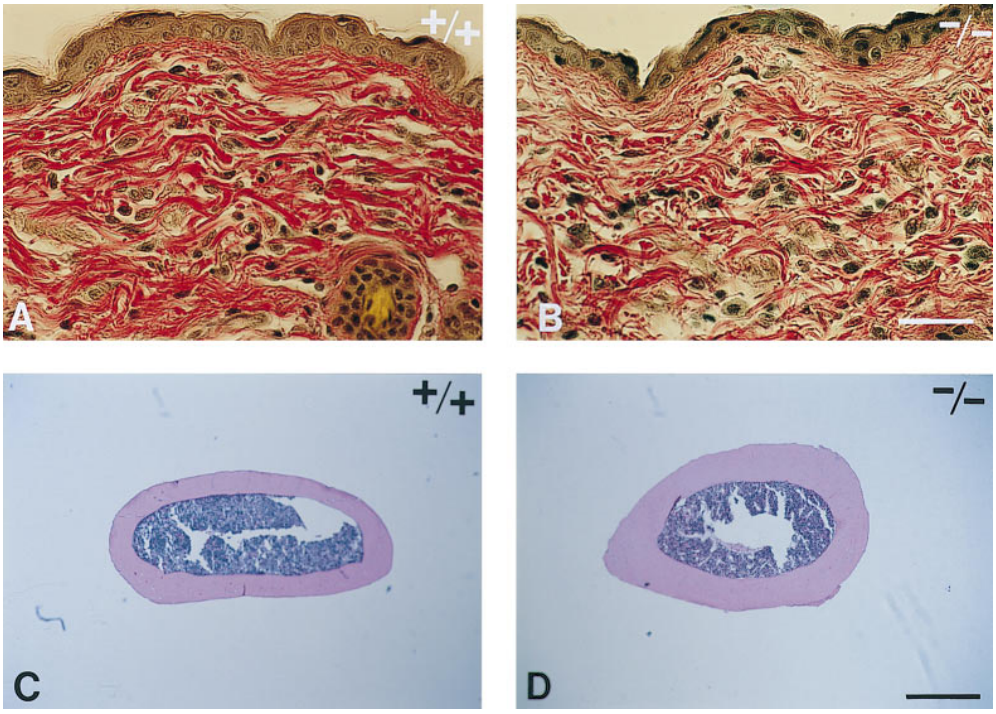

Figure 3. Histological analysis of skin and bone in the TSP2-null mouse. (*A* and *B*) Dermis from the back of a *Thbs2* +/+ mouse (*A*) and a *Thbs2* −/− mouse (*B*), stained with Verhoeff-van Gieson stain. Collagen fibers stain orange-red and epidermis, cells, and hair follicle stain yellow-brown. The collagen fibers in *A* form a wicker-like mesh but are largely oriented parallel to the epidermal surface. Collagen fibers in *B* appear disorganized and lack the predominant orientation parallel to the epidermal surface. Bar, 50 μm. (*C* and *D*) Mid-diaphyseal cross-section of the femur of a *Thbs2* +/+ mouse (*C*) and a *Thbs2* −/− mouse (*D*), stained with H & E. The increased cortical thickness and reduced marrow cavity of the femur from the mutant animal are evident. The less regularly oval contour, and tendency to form a ridge, is a feature of the abnormal bone. Bar, 500 μm.

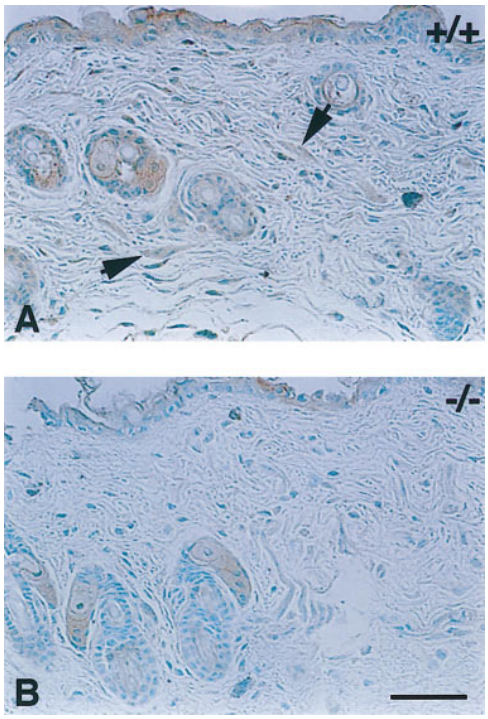

Figure 4. Immunohistochemical analysis for TSP-2 in back skin from (*A*) a *Thbs2*+/+ mouse and (*B*) a *Thbs2* −/− mouse. The sections were counterstained with methyl green. The presence of TSP2 immunoreactivity, observed as brown-black color, is evident in *A*. The arrows indicate dermal cells that appear to be positive for TSP2. Immunoreactivity to the epidermis, sweat glands, and hair follicles is, in part, nonspecific. Bar, 50 μm.

collagen fibers were evident in mutant tissue. Whereas skin from *Thbs2* +/+ mice had a regular network of collagen fibers that appeared relatively tightly packed and was predominantly oriented parallel to the surface (Fig. 3 *A*), collagen fibers in *Thbs2* −/− tissue were disorganized, more widely spaced, and lacked an orientation to the epidermis (Fig. 3 *B*). However, the abnormality in dermal collagen fibers was patchy and some areas appeared relatively normal (data not shown). Immunohistochemical analyses of skin demonstrated the presence of TSP2 in dermal cells of *Thbs2* +/+ mice, and its absence from the cells of knockout animals (Fig. 4), but it was not possible to determine, unequivocally, whether TSP2 was located in collagen fibers of control animals, or whether the small amount of reaction product in the control tissue that was apparently fiber associated was present in cellular processes or in the pericellular environment.

Electron microscopic examination of dermal collagen from the skin of *Thbs2* −/− mice revealed the presence of numerous fibrils that had uneven contours and were larger than normal (Fig. 5 *B*). The presence of these abnormal fibrils was limited largely to the reticular dermis and, as was seen by light microscopy, regions of abnormality were interspersed with more normal-appearing fibrils. In contrast, collagen fibrils in *Thbs2* +/+ mice were more uniform in size and had relatively even contours (Fig. 5 *A*). Cross-sectional profiles of collagen fibrils from areas selected as abnormal were analyzed morphometrically. The

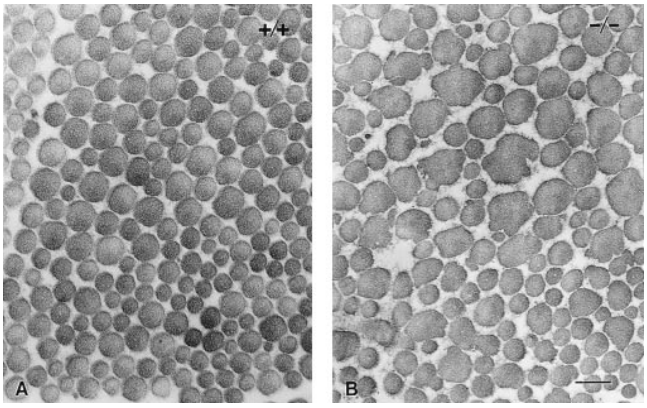

Figure 5. Electron micrographs of collagen fibrils in reticular dermis from a *Thbs2* +/+ mouse (*A*) and a *Thbs2* −/− mouse (*B*). The presence of larger fibrils with irregular contours in the tissue from the mutant animal, in comparison with the more uniformly sized circular fibrils in the control tissue, is evident. Bar, 250 nm.

results showed an average diameter of 145 ± 51 nm for the fibrils of *Thbs2* −/− mice, which is significantly greater ($P \leq 0.001$) than the average fibril diameter of 122 ± 23 nm in *Thbs2* +/+ mice (Fig. 6). It is of interest that findings intermediate between those in wild-type and mutant animals were observed in skin from heterozygous *Thbs2* +/− mice. Large fibrils were more numerous than in control tissue, but the contours of these fibrils were less irregular than those in TSP2-null animals (data not shown). Thus, at least in skin, there is haplo-insufficiency for the function of TSP2.

The impression of increased skin fragility in *Thbs2* −/− mice was confirmed by measurements of tensile strength. Fig. 7, *A* and *B*, show stress/displacement curves of skin obtained from the backs of *Thbs2* +/+ and *Thbs2* −/− mice. Identical portions of skin removed from decorin-null animals, known to exhibit a marked reduction in tensile strength, were studied concurrently as positive controls. The two panels describe curves obtained with specimens from different animals. In both experiments the curves for *Thbs2* −/− skin differed from those for *Thbs2* +/+ control samples in that (*a*) the break point of the mutant tissue was lower than that of the control (8 vs. 19 newtons in *A*; 9 vs. 13 newtons in *B*); (*b*) the ascending slopes of the curves for the *Thbs2* −/− tissue were less steep than those for the control tissue, indicative of greater displacement per unit increase in load, or increased elasticity (decreased elastic modulus) of the pathological material; (*c*) the break point of the *Thbs2* −/− samples occurred at a greater displacement than that of the normal controls and the curves showed a short plateau region, just before the break point, during which increasing displacement occurred without an increase in load. Both of these features are indicative of increased ductility. Altogether, duplicate skin strips from five *Thbs2* −/− and five *Thbs2* +/+ mice were tested. There was considerable variation in the load or force required to rupture the tissue, which is inherent in the method, and several analyses were excluded for technical reasons.On average, the mean point of failure for the two tissues was significantly different (*Thbs2* +/+: 11.9 ± 1.55

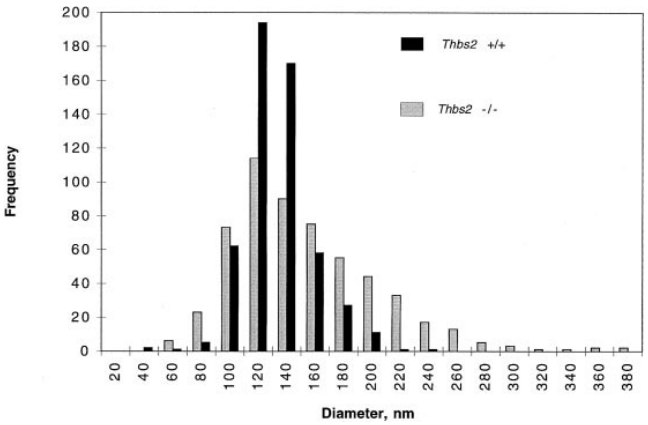

Figure 6. Distribution of collagen fibril diameters, as measured from electron micrographs of skin from *Thbs2* +/+ (*solid bars*) and *Thbs2* −/− (*shaded bars*) mice. The distribution is skewed in the direction of larger fibrils in the mutant tissue.

N (SEM), $n = 7$; *Thbs2* −/−: 8.7 ± 0.37 N (SEM), $n = 10$; $P \leq 0.07$).

Tails and Tail Tendons Are Abnormal in TSP2-null Mice

On close examination, *Thbs2* −/− mice were observed to drag their tails while scampering, indicating poor control of tail movement. The tail itself was highly flexible and contained a series of subtle bends, even in its resting state. The end of a mutant tail could be tied in a knot that was often maintained for some minutes (Fig. 2). This manipulation, which did not appear to distress the mouse, was impossible in the normal animal. When held by the tips of their tails, TSP2-null mice also had considerable difficulty in pulling their bodies up to the base of their tails, and the arcs of the stressed tails tended to be abnormal when compared to those of *Thbs2* +/+ mice. Thus, it would appear

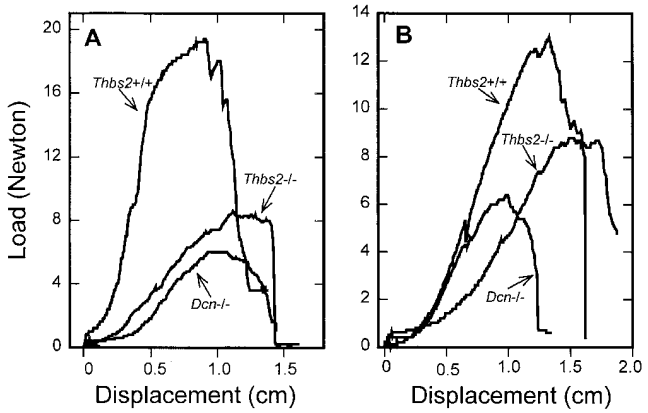

Figure 7. Measurements of tensile strength of skin from *Thbs2* +/+, *Thbs2* −/−, and decorin (*Dcn*) −/− mice. Force or load in newtons is plotted against displacement or elongation of skin in cm. *A* and *B* show experiments with tissues from different animals. In both, skin from TSP2-null mice ruptures at a lower load, and shows increased ductility (greater displacement per unit increase in load), than skin from control mice.

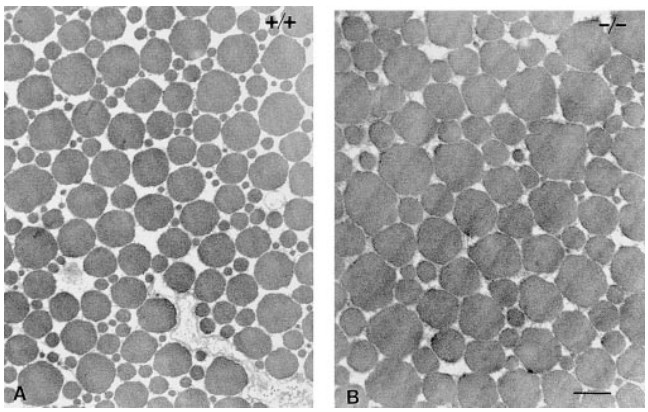

Figure 8. Electron micrographs of collagen fibrils in tendon from (*A*) a *Thbs2* +/+ mouse, and (*B*) a *Thbs2* −/− mouse. In *B*, larger fibrils are relatively more numerous than smaller fibrils and frequently display irregular contours. Small diameter fibrils in *A* represent tapered fibril ends and are much less frequent in *B*. Bar, 250 nm.

that the mice had abnormalities in tail tendons and in intervertebral ligaments.

Although light microscopic analysis of sagittal and cross-sections of tail tissue from *Thbs2* −/− mice did not show consistent abnormalities, examination of tail tendon from these mice by electron microscopy revealed the presence of abnormal collagen fibrils with greater than normal diameters and uneven contours (Fig. 8 *B*). Thus, in contrast to the diameters of large control tendon fibrils that were in the range of 250 nm (Fig. 8 *A*), the diameters of the largest fibrils in *Thbs2* −/− tendon were as high as 400 nm. Although we have not yet had the opportunity to examine ligaments in tail tissue in detail, the impression of increased laxity is supported by manual manipulation of skeletal preparations.

TSP2-null Skin Fibroblasts Do Not Adhere Normally to a Substratum

Skin fibroblasts were isolated from neonatal (1-d-old) and adult (3-mo-old) mice by explant culture of skin biopsies. The growth rates of cells derived from *Thbs2* +/+ and *Thbs2* −/− mice were approximately equal, and analysis of collagen synthesis revealed no significant differences between normal and mutant cells, as determined by SDS-PAGE of ^{3}H-labeled proteins in culture medium, before and after collagenase digestion (data not shown). However, the two cell populations differed in other growth characteristics and in adhesive properties. *Thbs2* −/− cells were less contact inhibited and assumed a multi-layered arrangement at confluence. In addition, adherent *Thbs2* −/− cells were more sensitive to trypsinization from tissue culture plastic, and their behavior differed from wild-type cells when plated on surfaces such as glass or bacteriological plastic. In contrast to *Thbs2* +/+ cells that remained dispersed as single cells or small clumps of cells after plating on bacteriological plastic (Fig. 9 *A*), aggregates of *Thbs2* −/− cells were observed within an hour (Fig. 9 *B*), and these aggregates grew in size with time, sometimes coalescing into a cell sheet. On tissue culture plastic, attach-

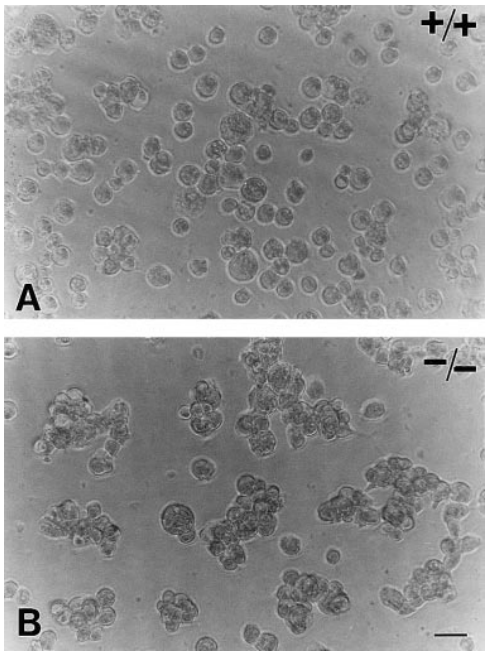

Figure 9. Appearance of neonatal skin fibroblasts isolated from *Thbs2* +/+ mice (*A*) and *Thbs2* −/− mice (*B*) 1 h after plating on bacteriologic plastic in DME. Control fibroblasts remain dispersed whereas fibroblasts from mutant mice form small aggregates that coalesce with time. Bar, 50 μm.

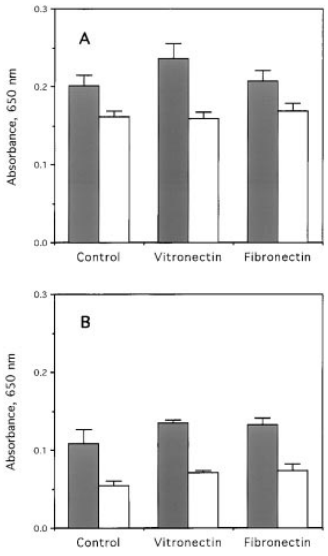

Figure 10. Fibroblast attachment assays. (*A*) Adult skin fibroblasts (2×10^5/ml) were plated, in the presence of DME plus 10% serum, on untreated (control) wells or on wells coated with vitronectin or fibronectin in a 96-well tissue culture plate, and allowed to attach for 1 h. Attached cells were quantitated spectrophotometrically by adsorbed methylene blue. (*B*) In a separate experiment, cells that did not attach under conditions such as those described in *A* were retested for their ability to attach under the same conditions. Shaded bars, *Thbs2* +/+ cells; open bars, *Thbs2* −/− cells. All differences are significant ($P \leq 0.05$).

ment of adult TSP2-null cells was reduced compared to normal cells (Fig. 10 *A*), and this difference was more apparent when cells that did not initially attach (~50%) were replated on the same substratum (Fig. 10 *B*). Coating of the surface with vitronectin or fibronectin did not correct the attachment defect (Fig. 10 *B*), nor did coating with TSP2 or type I collagen (not shown). We conclude that the defect in attachment of TSP2-null cells does not result from a lack of attachment factors or TSP2, but from changes in cell surface properties, possibly in adhesion receptors (see Discussion).

TSP2-null Mice Display Increased Cortical Bone Thickness and Density

The possibility of an abnormality in bone in TSP2-null mice was suggested by the distribution of TSP2 mRNA (Iruela-Arispe et al., 1993) and protein (Kyriakides, T.R., Y.-H. Zhu, and P. Bornstein, manuscript in preparation) at sites of chondrogenesis and osteogenesis during normal embryonic development. Examination of tibias and femurs from 3- and 5-mo-old mice by histology and pQCT revealed increased total bone density and cortical thickness. The mid-diaphyseal cross-sections of the 3-mo-old femurs shown in Fig. 3, *C* and *D*, are indicative of the increase in cortical bone thickness in the mutant mice. Five control and TSP2-null mice were analyzed by pQCT and the results of the tibial and femoral measurements are summarized in Table I. Although there is variation among normal animals and, as for skin and tendon, the mutant phenotype appears to be incompletely penetrant, the differences in total bone density and cortical thickness are statistically significant.

Other Abnormalities in TSP2-null Mice

TSP2-null mice display at least two other abnormalities. Mutant mice have an abnormally long bleeding time, as judged by the length of time it takes for a tail wound to stop bleeding. Mice were restrained in a simple device and a 1-cm segment of tail was cut from the tip. The average time for spontaneous cessation of bleeding in normal mice was 2.2 min ($n = 5$). Of the five TSP2-null mice, three continued to bleed beyond 10 min and required intervention. The other two mice had bleeding times of 7.5 and 8.5 min. Clotting parameters were normal in mutant mice. Specifically, the prothrombin and partial thromboplastin times were 11.5 and 38 s, respectively, for *Thbs2* −/− mice ($n = 5$), and 11.9 and 46 s, respectively, for *Thbs2* +/+ mice ($n = 2$). The platelet count of TSP2-null mice was $7.46 \times 10^5/\mu l \pm 5.8 \times 10^4$ (SD), $n = 5$, which is significantly higher than that in wild-type animals (5.99×10^5/ml ± 6.47 x 10^4 (SD), $n = 5$; $P \leq 0.005$).

TSP2-null mice also have a striking increase in the density of small- and medium-sized blood vessels in many tissues. This characteristic was noticed first as an increase in erythrocyte-containing structures in H & E- and Verhoeff-van Gieson–stained sections of skin. Sections of adult,

Table I. Quantification of Total Bone Density and Cortical Thickness in TSP2-null and Wild-type Mice

	Femur		Tibia	
	Total Density	Cortical Thickness	Total Density	Cortical Thickness
Thbs2 +/+	450.5 ± 25	0.26 ± 0.016	480.8 ± 34.3	0.238 ± 0.031
Thbs2 −/−	498.5 ± 24	0.29 ± 0.017	538.1 ± 31.6	0.275 ± 0.013
	$P \leq 0.05$	$P \leq 0.05$	$P \leq 0.05$	$P \leq 0.05$

The total bone density of the femur and tibia (expressed as mg/cm^3) was determined by quantitative computerized tomography of the bone at mid-diaphysis. Cortical bone thickness, (in mm) at mid-diaphysis, was calculated from computer-generated algorithms based on cross-sectional geometries. Values represent mean ± SEM; $n = 5$ for all values.

Table II. Quantification of Blood Vessels in Tissue Sections

Tissue	Blood vessels per 40× field*	
	Thbs2 +/+	*Thbs2* −/−
Adult adipose	7.4 ± 1.2‡	17.3 ± 2.3
Embryonic adipose	9.7 ± 3.1	17.2 ± 5.6
Adult dermis	5.1 ± 2.0	10.0 ± 2.4
Neonatal dermis	8.9 ± 2.8	12.9 ± 2.8
Embryonic dermis	18.8 ± 2.2	22.5 ± 3.5
Embryonic thymus	13.1 ± 1.5	22.9 ± 2.4

*Sections were imunostained with an antibody to vWF. Counts are the averages of 7–20 40× microscopic fields (0.075 mm^2/field) obtained by examination of 6 μm sections from four control and three mutant mice.
‡Standard deviation. All differences between sections from TSP2 +/+ and TSP2 −/− mice are significant at a level of $P \leq 0.001$, with the exception of embryonic dermis for which the level of significance is $P \leq 0.04$.

neonatal, and embryonic dermis, adult and embryonic subcutaneous adipose tissue, and embryonic thymus were immunostained with an antibody to vWF, and endothelial cell–containing vascular structures were counted by an investigator who had no knowledge of the genotype of the tissue. The results are summarized in Table II. On average, there were twice as many blood vessels in a 40× microscopic field (0.075 mm^2) in sections from adult mutant mice, compared with those from control animals, and all comparisons were different with a high degree of statistical significance. Interestingly, the differences for neonatal and embryonic dermis were not as great as those for the adult tissue. Representative sections of neonatal dermis from *Thbs2* +/+ and *Thbs2* −/− mice, stained for vWF, are shown in Fig. 11.

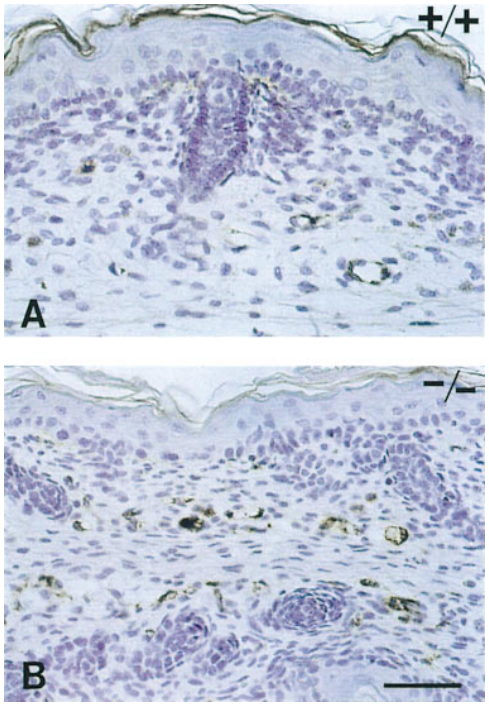

Figure 11. Immunohistochemical analysis for vWF of back skin from (*A*) a *Thbs2* +/+ mouse and (*B*) a *Thbs2* −/− mouse. The sections were counterstained with hematoxylin. These sections are representative of those reported in Table II and show the increased vascular density in TSP2-null mice. Bar, 50 μm.

Discussion

The Phenotype of the TSP2-null Mouse

The TSP2-null mouse is normal in size and appearance and reproduces normally. To the trained investigator, however, these mice are distinctive. Juvenile mice often have subtle bends in their tails that tend to become less distinct as they mature. The skin of adult mice feels more stretchable and the tail is clearly more flexible, as evidenced by the ability to fashion knots in it (Fig. 2). These overt indications of abnormalities in connective tissue structure and function are supported by anatomical analysis and mechanical testing. The weave of dermal collagen fibers in the TSP2 knockout mouse is disorganized (Fig. 3 *B*), and collagen fibrils in skin and tendon are abnormally large and irregularly contoured when examined by electron microscopy (Figs. 5, 6, and 8). Tensile strength measurements of skin from mutant animals support indications of increased fragility, first suggested by the tendency of skin to tear. Skin from TSP2-null mice ruptures at lower loads and has increased ductility (Fig. 7); these findings explain its increased stretchability. A possible clue to the pathogenesis of these disorders lies in the abnormalities of attachment documented in skin fibroblasts from mutant animals (Figs. 9 and 10). TSP2-null mice also show an increase in cortical bone width (Fig. 3, *C* and *D*). Finally, mutant mice have a significant increase in density in small blood vessels in skin and other tissues, and an abnormally long bleeding time.

It should be emphasized that there was considerable variability in the extent to which these various abnormalities were expressed in individual *Thbs2* −/− mice. This variability probably reflects, in part, the mixed genetic background (129/SvJ and C57BL/6) of the mice. It is now well established that genetic background can have a significant impact on the expression of a knockout phenotype (see Bonyadi et al., 1997 as a recent example relating to TGFβ1 knockout mice). We have transferred the TSP2 mutation to a pure 129 background, and have confirmed the major features of the phenotype, but have not yet determined whether the variability in the phenotype is reduced.

What Is the Basis for the Disordered Collagen Fibrils in TSP2-null Mice?

In vitro, homotypic collagen fibril formation is an entropy-driven, self-assembly process (Kadler et al., 1996). However, the situation in vivo is more complex. The presence of fibril-associated collagens and other macromolecules together with type I collagen in heterotypic fibrils affects properties such as form and diameter (Birk and Linsenmayer, 1994). Thus, Marchand et al. (1996) have used a dominant-negative strategy, involving the retroviral transduction of corneal fibroblasts with a truncated α1(V) minigene, to show by inference that the presence of type V collagen reduces the diameter of type I collagen fibrils. A requirement for type V collagen in collagen fibrillogenesis was shown definitively in mice by targeting a mutation to the *Col5A2* gene. Homozygous α2(V) mutant mice demonstrated a severe skin fragility, and corneal collagen fibrils

were reported to be wider than normal (Andrikopoulos et al., 1995). Similarly, the decorin knockout mouse was recently reported (Danielson et al., 1997) to have fragile skin with larger, irregularly contoured collagen fibrils that resemble, in some respects, the fibrils seen in the TSP2 knockout mouse. We have examined the skin of *Thbs2* −/− and control mice by histochemical analysis with antidecorin antibodies (a gift of L. Fisher, National Institute of Dental Research, National Institutes of Health, Bethesda, MD) and found no difference in the level of staining (our unpublished results).

The presence of skin fragility and abnormal collagen fibrils in the TSP2 and decorin knockout mice, and in the α2(V) mutant mouse, raise the possibility that, like type V collagen and decorin, TSP2 might function as a collagen fibril-associated protein that regulates fibril diameter and fibrillogenesis. Although, to our knowledge, the binding of TSP2 to collagens has not been studied, TSP1 has been shown to bind to a number of collagens including types I and V (Mumby et al., 1984; Galvin et al., 1987). Binding was dependent on the native conformation of the collagen and involved a chymotrypsin-resistant fragment of TSP1 (Mumby et al., 1984), that is now known to include the procollagen homology domain and type I repeats (Galvin et al., 1987). Because of similarities of amino acid sequence between TSP1 and TSP2 in these regions of the proteins (Bornstein, 1992; Laherty et al., 1992), it is likely that TSP2 will also be found to bind types I and V collagens, but whether TSP2 functions as a fibril-associated protein is not known. Immunohistochemical analysis of skin with anti-TSP2 antibodies (Fig. 4) suggests the presence of some staining in control tissue that is not obviously within cells, but whether or not this reaction product represents TSP2 that is specifically associated with collagen fibrils will require examination at the ultrastructural level.

It has been suggested that fibroblasts compartmentalize the adjacent extracellular space to enable fibrils to assemble in deep crevasses or channels, largely surrounded by the cell surface (Birk and Trelstad, 1986; Ploetz et al., 1991; Birk and Linsenmayer, 1994). The process of fibril growth is presumed to occur by retraction of cell processes and lateral aggregation of fibrils. In view of the defect that we have identified in the attachment properties of skin fibroblasts from TSP2-null mice (Figs. 9 and 10) it seems possible that an alternative or additional explanation for the disordered collagen fibrillogenesis in these mice reflects the altered cell surface properties of fibroblastic cells, and their inability to interact normally with collagen fibrils.

Skin Fibroblasts from TSP2-null Mice Display a Defect in Attachment to a Substratum

In vitro, fibroblasts are capable of interacting, by means of integrins and nonintegrin cell surface receptors, to a variety of extracellular matrix proteins, including fibronectin, collagens, and laminins, and to matricellular proteins such as TSP1 and TSP2, tenascins, and secreted protein acidic, and rich in cysteine (SPARC). In some studies, attachment of human embryonic fibroblasts to TSP1 was shown to lead rapidly to spreading and to the formation of focal adhesions that were mediated by a number of receptors, including $\alpha_v\beta_3$ integrin and CD36 (Stomski et al., 1992). However, in the case of endothelial cells, smooth muscle cells, and myoblasts, TSP1, and probably TSP2, inhibit the formation of focal contacts, and these proteins are also capable of destabilizing focal adhesions formed by adhesive proteins such as fibronectin (Murphy-Ullrich and Höök, 1989; Murphy-Ullrich et al., 1993; Sipes et al., 1993; Adams, 1995; Murphy-Ullrich et al., 1996). We have found that skin fibroblasts from TSP2-null mice attach more poorly to tissue culture plastic than do control fibroblasts, and that this defect cannot be corrected by plating the cells on a number of matrix proteins, including TSP2. In preliminary studies we have also found that TSP2-null cells do not contract a collagen gel normally (our unpublished results). These findings suggest that TSP2 functions as a proadhesive protein for fibroblasts, but that the basis for the attachment defect in cells lacking TSP2 is not simply the absence of a suitable substratum.

How Might a Lack of TSP2 Cause an Increase in Bone Density?

An increase in bone density in mice and humans most commonly results from reduced resorption of bone by osteoclasts, a condition which is termed osteopetrosis (Popoff and Marks, 1995). In mice, osteoclast function can be compromised either metabolically, e.g., by targeted disruption of the gene encoding tartrate-resistant acid phosphatase (Hayman et al., 1996), or by a block in differentiation of osteoclast precursor cells. Not all increases in bone density involve osteoclasts, as the bone defect in the osteocalcin-deficient mouse results from an increase in bone formation rather than from an impairment in bone resorption (Ducy et al., 1996). Histomorphometric studies are currently in progress to determine whether changes in bone formation or resorption are operative in TSP2-null mice. If the latter mechanism is implicated, the bone defect in TSP2-null mice could result from a defect in osteoclast adhesion to bone, or from a failure to form a bone-resorbing ruffled border. The origin of this putative defect may have parallels with the attachment defect that we have begun to investigate in skin fibroblasts. Alternatively, the differentiation of osteoclast precursors in the marrow could be affected by abnormalities in the stromal matrix or in stromal-precursor cell interactions.

The Bleeding Diathesis and Vascular Abnormality in TSP2-null Mice

Although platelet α granules contain abundant TSP1 (McGregor and Boukerche, 1993), there is no evidence for the presence of TSP2 in platelets. Indeed, *Thbs1* mRNA, but not *Thbs2* mRNA, is readily detected by in situ hybridization in hematopoietic precursor cells in developing mouse embryo liver, spleen, and bone marrow (Iruela-Arispe et al., 1993). Similarly, TSP1 but not TSP2, can be detected by Western analysis of adult mouse serum (our unpublished observations). Provided platelet function can be shown to be normal, the most probable cause of the bleeding diathesis in TSP2-null mice is defective adhesion of platelet aggregates to the injured subendothelium. The role of vWF in anchoring aggregated platelets to the subendothelium is well established, and mutations in the vWF gene are a common cause of bleeding disorders in humans

(Sadler, 1995), but the nature of the interaction between vWF and the subendothelium is still not well understood (Sixma and deGroot, 1994; Weiss, 1995). There is evidence that collagen types I, III, IV, and VI and fibronectin may be involved in mediating platelet adhesion (Houdijk et al., 1986; Weiss, 1995). TSP1 has been shown to bind to vWF (Mumby et al., 1984; Barabino et al., 1997), and it is not unreasonable to suggest that this will also be true for TSP2. In view of the derangement of collagen fibrillogenesis in TSP2-null mice, it seems possible that TSP2 is required, either directly or indirectly, for the binding of vWF to one or more collagens in the subendothelium.

The increase in blood vessel density in TSP2-null mice is indubitable (Table II), and this finding provides, we believe, the strongest argument yet presented for the function of a thrombospondin as an inhibitor of angiogenesis in vivo. TSP2 has been shown to inhibit the migration of bovine adrenal capillary endothelial cells in a modified Boyden chamber, and to inhibit basic FGF-induced neovascularization in the rat cornea (Volpert et al., 1995). With the exception of this study, all previously published work on the role of TSPs in angiogenesis has involved TSP1 and this work has generated considerable controversy (for reviews see Roberts, 1996; Tuszynski and Nicosia, 1996; Bouck, 1996; and Bouck et al., 1996). Based on a reading of the literature, one reaches the conclusion that whereas TSP1 can be considered to be antiangiogenic in assays involving endothelial migration or corneal neovascularization, the situation in vivo might be more complex. A resolution of conflicting findings may lie in recognition of the diversity of function inherent in matricellular proteins such as TSP1 (Bornstein, 1995). In addition to its intrinsic ability to modulate angiogenesis by variably affecting the adhesion, migration, and proliferation of endothelial cells (see reviews above), TSP1 can bind basic FGF (Taraboletti et al., 1997), which could either present or sequester this potent proangiogenic growth factor. TSP1 could also recruit cells whose net effect would be proangiogenic, as postulated by Nicosia and Tuszynski (1994) in their rat aortic ring culture model. Although the detailed phenotype of the TSP1 knockout mouse has not been published, Stellmach et al. (1996) reported that TSP1-null mice have an increase in blood vessels in the anterior and posterior chambers of the eye, but presumably not a generalized increase in vascular density. Because these tissue compartments are relatively isolated from invasion by cells in adjacent tissues, it is possible that the absence of TSP1 could tilt the balance of pro- and antiangiogenic factors in favor of the former. On the other hand, the activities of TSP2 may be more purely antiangiogenic if, for example, the protein is less capable of recruiting cells from adjacent sites, which could contribute an angiogenic effect. As a result, the lack of TSP2 would lead to the more generalized increase in vascular density that we have observed in the TSP2 knockout mouse.

Conclusions

The phenotype of the TSP2-null mouse implicates TSP2 in collagen fibrillogenesis, bone growth, maintenance of a normal vascular density, hemostasis, and in the attachment properties of skin fibroblasts and perhaps other cells. With the possible exception of the vascular effect, none of these findings could have been predicted from the known functions of TSP1 or TSP2. This study, therefore, makes a strong argument for the use of gene targeting as a means of assessing biological function, although there are certainly many instances in which overlapping functions or gene compensation can obscure the function of a missing protein (Bornstein, 1995; Hynes, 1996). The striking defect in collagen fibrils in skin and tendon of TSP2-null mice suggests that TSP2 may function as a fibril-associated structural component in these tissues. However, an equally plausible explanation can be provided by postulating a defect in cell surface properties of fibroblasts. Although, at first glance, the finding of an attachment defect in fibroblasts from TSP2-null mice would appear to contradict the report that the protein functions to reduce focal adhesions in endothelial and smooth muscle cells (Murphy-Ullrich et al., 1993), this conclusion is not necessarily justified. TSP2, through its interaction with multiple cell surface receptors and the consequent generation of intracellular signals, may be responsible for a variety of cell surface properties, the loss of which characterize the TSP2-null fibroblast. Therefore, a comparison cannot be readily made between the behavior of a cell that is deficient in an extracellular protein and that of a normal cell to which an excess of that protein is added. For a similar reason, one would not expect the addition of TSP2 to TSP2-null fibroblasts to correct functional defects in short term experiments. We believe that the TSP2-null mouse and its cells represent a unique and valuable resource for studies of matrix synthesis and assembly, angiogenesis, bone growth, and hemostasis.

We thank Patricia Jun, Kim Yeargin, Deb Puerner, and Martha Strachan for technical assistance, Sean Kim for assistance with animal husbandry, Christina King for assistance with blastocyst injections, and Helene Sage and members of our laboratories for valuable discussions and a critical reading of the manuscript. P. Bornstein is indebted to Hong Wu, Xin Liu, and Rudolf Jaenisch for assistance with gene targeting during the early phases of this work. D. Mosher, L. Fisher, and R. Jaenisch contributed valuable reagents.

This work was supported by National Institutes of Health grants P01 HL18645 and DE08229 (P. Bornstein), and AR21557 (L. Smith), and by National Science Foundation grant ECC9529161 (P. Bornstein and L. Smith).

Received for publication 14 August 1997 and in revised form 7 November 1997.

References

Adams, J.C. 1995. Formation of stable microspikes containing actin and the 55 kda actin bundling protein, fascin, is a consequence of cell adhesion to thrombospondin-1: implications for the anti-adhesive activities of thrombospondin-1. *J. Cell Sci.* 108:1977–1990.

Adams, J.C., and J. Lawler. 1993. Diverse mechanisms for cell attachment to platelet thrombospondin. *J. Cell Sci.* 104:1061–1071.

Andrikopoulos, K., X. Liu, D.R. Keene, R. Jaenisch, and F. Ramirez. 1995. Targeted mutation in the Col5α2 gene reveals a regulatory role for type V collagen during matrix assembly. *Nat. Genet.* 9:31–36.

Aumailley, M., K. Mann, H. von der Mark, and R. Timpl. 1989. Call attachment properties of collagen type VI and Arg-Gly-Asp dependent binding to its α2(VI) and α3(VI) chains. *Exp. Cell Res.* 181:463–474.

Barabino, G.A., R.J. Wise, V.A. Woodbury, B.B. Zhang, K.A. Bridges, R.P. Hebbel, J. Lawler, and B.M. Ewenstein. 1997. Inhibition of sickle erythrocyte adhesion to immobilized thrombospondin by von willebrand factor under dynamic flow conditions. *Blood.* 89:2560–2567.

Birk, D.E., and R.L. Trelstad. 1986. Extracellular compartments in tendon morphogenesis: collagen fibril, bundle, and macroaggregate formation. *J. Cell Biol.* 103:231–240.

Birk, D.E., and T.F. Linsenmayer. 1994. Collagen fibril assembly, deposition,

and organization into tissue-specific matrices. *In* Extracellular Matrix Assembly and Structure. P.D. Yurchenco, D.E. Birk, and R.P. Mecham, editors. Academic Press, San Diego, CA. 91–128.

Bonyadi, M., S.B. Rusholme, F.M. Cousins, H.C. Su, C.A. Biron, M. Farrall, and R.J. Akhurst. 1997. Mapping of a major genetic modifier of embryonic lethality in TGFβ1 knockout mice. *Nat. Genet.* 15:207–211.

Bornstein, P. 1992. The thrombospondins: structure and regulation of expression. *FASEB (Fed. Am. Soc. Exp. Biol.) J.* 6:3290–3299.

Bornstein, P. 1995. Diversity of function is inherent in matricellular proteins: an appraisal of thrombospondin 1. *J. Cell Biol.* 130:503–506.

Bornstein, P., and E.H. Sage. 1994. Thrombospondins. *Methods Enzymol.* 245: 62–85.

Bornstein, P., S. Devarayalu, P. Li, C.M. Disteche, and P. Framson. 1991*a.* A second thrombospondin gene in the mouse is similar in organization to thrombospondin 1 but does not respond to serum. *Proc. Natl. Acad. Sci. USA.* 88:8636–8640.

Bornstein, P., K. O'Rourke, K. Wikstrom, F.W. Wolf, R. Katz, P. Li, and V.M. Dixit. 1991*b.* A second, expressed thrombospondin gene (*Thbs2*) exists in the mouse genome. *J. Biol. Chem.* 266:12821–12824.

Bouck, N. 1996. P53 and angiogenesis. *Biochim. Biophys. Acta.* 1287:63–66.

Bouck, N., V. Stellmach, and S.C. Hsu. 1996. How tumors become angiogenic. *Adv. Cancer Res.* 69:135–174.

Burrows, N.P., A.C. Nicholls, J.R.W. Yates, G. Gatward, P. Sarathachandra, A. Richards, and F.M. Pope. 1996. The gene encoding collagen α1(V) (COL5A1) is linked to mixed Ehlers-Danlos Syndrome type I/II. *J. Investig. Dermatol.* 106:1273–1276.

Byers, P.H. 1995. Disorders of collagen biosynthesis and structure. *In* The Metabolic and Molecular Bases of Inherited Disease. C.R. Scriver, A.L. Beaudet, W.S. Sly, and D. Valle, editors. McGraw-Hill, Inc., New York. 4029–4077.

Chen, H., D.K. Strickland, and D.F. Mosher. 1996. Metabolism of thrombospondin 2: binding and degradation by 3T3 cells and glycosaminoglycan-variant chinese hamster ovary cells. *J. Biol. Chem.* 271:15993–15999.

Chen, H., J. Sottile, K.M. O'Rourke, V.M. Dixit, and D.F. Mosher. 1994. Properties of recombinant mouse thrombospondin 2 expressed in Spodoptera cells. *J. Biol. Chem.* 269:32226–32232.

Chomczynski, P., and N. Sacchi. 1987. Single-step method of RNA isolation by acid guanidium thiocyanate-phenolchloroform extraction. *Anal. Biochem.* 162:156–159.

Danielson, K.G., H. Baribault, D.F. Holmes, H.Graham, K.E. Kadler, and R.V. Iozzo. 1997. Targeted disruption of decorin leads to abnormal collagen fibril morphology and skin fragility. *J. Cell Biol.* 136:729–743.

Ducy, P., C. Desbois, B. Boyce, G. Pinero, B. Story, C. Dunstan, E. Smith, J. Bonadio, S. Goldstein, C. Gundberg, A. Bradley, and G. Karsenty. 1996. Increased bone formation in osteocalcin-deficient mice. *Nature.* 382:448–452.

Frazier, W.A. 1991. Thrombospondins. *Curr. Opin. Cell Biol.* 3:792–799.

Galvin, N.J., P.M. Vance, V.M. Dixit, B. Fink, and W.A. Frazier. 1987. Interaction of human thrombospondin with types I-V collagen: Direct binding and electron microscopy. *J. Cell Biol.* 104:1413–1422.

Hayman, A.R., S.J. Jones, A. Boyde, D. Foster, W.H. Colledge, M.B. Carlton, M.J. Evans, and T.M. Cox. 1996. Mice lacking tartrate-resistant acid phosphatase (Acp 5) have disrupted endochondral ossification and mild osteopetrosis. *Development.* 122:3151–3162.

Houdijk, W.P.M., P.G. de Groot, P.F.E.M. Nievelstein, K.S. Sakariassen, and J.J. Sixma. 1986. Subendothelial proteins and platelet adhesion. von Willebrand factor and fibronectin, not thrombospondin, are involved in platelet adhesion to extracellular matrix of human vascular endothelial cells. *Arteriosclerosis.* 6:24–33.

Hynes, R.O. 1996. Targeted mutations in cell adhesion genes: what have we learned from them? *Dev. Biol.* 180:402–412.

Iozzo, R.V., and A.D. Murdoch. 1996. Proteoglycans of the extracellular environment: clues from the gene and protein side offer novel perspectives in molecular diversity and function. *FASEB (Fed. Am. Soc. Exp. Biol.) J.* 10: 598–614.

Iruela-Arispe, M.L., D.J. Liska, E.H. Sage, and P. Bornstein. 1993. Differential expression of thrombospondin 1, 2, and 3 during murine development. *Dev. Dyn.* 197:40–56.

Kadler, K.E., D.F. Holmes, J.A. Trotter, and J.A. Chapman. 1996. Collagen fibril formation. *Biochem. J.* 316:1–11.

Lafeuillade, B., S. Pellerin, M. Keramidas, M. Danik, E.M. Chambaz, and J.J. Feige. 1996. Opposite regulation of thrombospondin-1 and corticotropin-induced secreted protein/thrombospondin-2 expression by adrenocorticotropic hormone in adrenocortical cells. *J. Cell. Physiol.* 167:164–172.

Laherty, C.D., K. O'Rourke, F.W. Wolf, R. Katz, M.F. Seldin, and V. M. Dixit. 1992. Characterization of mouse thrombospondin 2 sequence and expression during cell growth and development. *J. Biol. Chem.* 267:3274–3281.

Laird, P.W., A. Zijderveld, K. Linders, M.A. Rudnicki, R. Jaenisch, and A. Berns. 1991. Simplified mammalian DNA isolation procedure. *Nucleic Acids Res.* 19:4153.

Liu, X., H. Wu, M. Byrne, S. Krane, and R. Jaenisch. 1997. Type III collagen is crucial for collagen I fibrillogenesis and for normal cardiovascular development. *Proc. Natl. Acad. Sci. USA.* 94:1852–1856.

Marchant, J.K., R.A. Hahn, T.F. Linsenmayer, and D.E. Birk. 1996. Reduction of type V collagen using a dominant-negative strategy alters the regulation of fibrillogenesis and results in the loss of corneal-specific fibril morphology. *J. Cell Biol.* 135:1415–1426.

McGregor, J.L., and H. Boukerche. 1993. Thrombospondin interaction with human blood platelets. *In* Thrombospondin. J. Lahav, editor. CRC Press, Boca Raton, FL. 111–127.

Mumby, S.M., G.J. Raugi, and P. Bornstein. 1984. Interactions of thrombospondin with extracellular matrix proteins: selective binding to type V collagen. *J. Cell Biol.* 98:646–652.

Murphy-Ullrich, J.E. and M. Höök. 1989. Thrombospondin modulates focal adhesions in endothelial cells. *J. Cell Biol.* 109:1309–1319.

Murphy-Ullrich, J.E., S. Gurusiddappa, W.A. Frazier, and M. Höök. 1993. Heparin-binding peptides from thrombospondins 1 and 2 contain focal adhesion-labilizing activity. *J. Biol. Chem.* 268:26784–26789.

Murphy-Ullrich, J.E., M.A. Pallero, N. Boerth, J.A. Greenwood, T.M. Lincoln, and T.L. Cornwell. 1996. Cyclic GMP-dependent protein kinase is required for thrombospondin and tenascin mediated focal adhesion disassembly. *J. Cell Sci.* 109:2499–2508.

Nicosia, R.F., and G.P. Tuszynski. 1994. Matrix-bound thrombospondin promotes angiogenesis in vitro. *J. Cell Biol.* 124:183–193.

Pellerin, S., B. Lafeuillade, E.M. Chambaz, and J.J. Feige. 1994. Distinct effects of thrombospondin-1 and CISP/thrombospondin-2 on adrenocortical cell spreading. *Mol. Cell. Endocrinol.* 106:181–186.

Ploetz, C., E.I. Zycband, and D.E. Birk. 1991. Collagen fibril assembly and deposition in the developing dermis: segmental deposition in extracellular compartments. *J. Struct. Biol.* 106:73–81.

Popoff, S.N., and S.C. Marks. 1995. The heterogeneity of the osteopetroses reflects the diversity of cellular influences during skeletal development. *Bone.* 17:437–445.

Roberts, D.D. 1996. Regulation of tumor growth and metastasis by thrombospondin-1. *FASEB (Fed. Am. Soc. Exp. Biol.) J.* 10:1183–1191.

Sadler, J.E. 1995. von Willebrand disease. *In* The Metabolic and Molecular Bases of Inherited Disease. C.R. Scriver, A.L. Beaudet, W.S. Sly, and D. Valle, editors. McGraw-Hill Inc., New York. 3269–3287.

Sherbina, N.V., and P. Bornstein. 1992. Modulation of thrombospondin gene expression during osteoblast differentiation in MC3T3-E1 cells. *Bone.* 13: 197–201.

Sipes, J.M., N.H. Guo, E. Negre, T. Vogel, H.C. Krutzsch, and D.D. Roberts. 1993. Inhibition of fibronectin binding and fibronectin-mediated cell adhesion to collagen by a peptide from the 2nd type-I repeat of thrombospondin. *J. Cell Biol.* 121:469–477.

Sixma, J.J., and P.G. de Groot. 1994. Regulation of platelet adhesion to the vessel wall. *Ann. NY Acad. Sci.* 714:190–199.

Smith, L.T., U. Schwarze, J. Goldstein, and P.H. Byers. 1997. Mutations in the COL3A1 gene result in the Ehlers-Danlos Syndrome type IV and alterations in the size and distribution of the major collagen fibrils of the dermis. *J. Investig. Dermatol.* 108:241–247.

Stellmach, V., O.V. Volpert, S.E. Crawford, J. Lawler, R.O. Hynes, and N. Bouck. 1996. Tumour suppressor genes and angiogenesis: the role of TP53 in fibroblasts. *Eur. J. Cancer.* 32*A*:2394–2400.

Stomski, F.C., J.S. Gani, R.C. Bates, and G.F. Burns. 1992. Adhesion to thrombospondin by human embryonic fibroblasts is mediated by multiple receptors and includes a role for glycoprotein 88 (CD36). *Exp. Cell Res.* 198:85–92.

Taraboletti, G., D. Belotti, P. Borsotti, V. Vergani, M. Rusnati, M. Presta, and R. Giavazzi. 1997. The 140-kilodalton antiangiogenic fragment of thrombospondin-1 binds to basic fibroblast growth factor. *Cell Growth Differ.* 8:471–479.

Tucker, R.P. 1993. The in situ localization of tenascin splice variants and thrombospondin 2 mRNA in the avian embryo. *Development.* 117:347–358.

Tuszynski, G.P., and R.F. Nicosia. 1996. The role of thrombospondin-1 in tumor progression and angiogenesis. *Bioessays.* 18:71–76.

Vogel, A., K.A. Holbrook, B. Steinmann, R. Gitzelmann, and P.H. Byers. 1979. Abnormal collagen fibril structure in the gravis form (type I) of the Ehlers-Danlos syndrome. *Lab. Invest.* 40:201–206.

Volpert, O.V., S.S. Tolsma, S. Pellerin, J. Feige, H. Chen, D.F. Mosher, and N. Bouck. 1995. Inhibition of angiogenesis by thrombospondin-2. *Biochem. Biophys. Res. Commun.* 217:326–332.

Weiss, H.J. 1995. Flow-related platelet deposition on subendothelium. *Thromb. Haemostasis.* 74:117–122.